Int J Adv Manuf Technol (2017) 91:3061–3078
DOI 10.1007/s00170-016-9975-4

ORIGINAL ARTICLE

An investigation on enhancing ceramic shell properties using naturally available additives

Sarojrani Pattnaik [1]

Received: 19 July 2016 / Accepted: 26 December 2016 / Published online: 14 January 2017

Abstract The ceramic shell properties are very crucial in investment casting (IC) process. Colloidal silica based ceramic shells usually lack sufficient shell properties which causes shell cracking. Sometimes minor repairs can make up the shells. However, every time shell repairing may not be feasible which causes loss to the manufacturer. In the present work, an investigation has been made to improve the properties of colloidal silica based IC ceramic shell by addition of naturally available products such as saw dust and coconut fibres into the ceramic slurries. The important shell properties tested were shell thickness, green and fired strengths, porosity and permeability. The properties of saw dust and coconut fibre modified shells were compared with that of conventional ceramic shell using statistical analysis and it was found that the new shells were better than the conventional shell in terms of shell properties. Further, it was found that the aluminium alloy casting obtained from new shells showed comparatively increase in tensile strength and reduced porosity with that obtained from the conventional ceramic shell. The adopted method proved effective in reducing both production lead time and cost of manufacturing the qualitative IC ceramic shells.

Keywords Fibres · Porosity · Strength · Casting

Abbreviations

IC	Investment Casting
P-Type	Liquid polymer modified
C-Type	Coconut fibre modified
S-Type	Saw dust modified
Sec	Secondary layer
NCS	Nano-based Colloidal Sillica
MOR	Modulus of Rupture
AP	Apparent Porosity of ceramic shell
AP_{cast}	Apparent Porosity of casting
μ	Dynamic viscosity of air
r_i	Inner radius of the ceramic shell
r_o	Outer radius of the ceramic shell
P_i	Inner pressure of shell sample
P_o	Outer pressure of shell sample

✉ Sarojrani Pattnaik
rani_saroj7@yahoo.co.in

[1] Mechanical Engg. Department, Veer Surendra Sai University of Technology, Burla 768018, India

1 Introduction

Investment Casting (IC) is known for its precise production of parts such as turbine blades, airfoils, medical implants, dental parts, jewellery, etc. [1, 2]. The parts manufactured by this process possess superb surface finish with close dimensional tolerance [3]. The process usually involves building of ceramic layers of desired thickness around a disposable pattern so as to obtain a hollow ceramic shell on pattern removal. The shell is baked at high temperature to remove any traces of impurities present in it and then, it is filled with molten alloy at heated condition. On solidification of the molten alloy, the shell is ruptured to remove the casting out from it [4].

The construction of the ceramic shell is the most important stage of the IC process and the accuracy of the complex shaped parts require accurately dimensioned ceramic shells [5]. The shell should possess properties such as sufficient green or unfired strength to withstand the pressure during pattern removal, sufficient fired strength to resist the weight of the hot molten alloy, good breakability in order to remove the casting safely without being damaged, adequate porosity

and permeability to make the passage for the hot gases evolved during melting of the alloy to move outside the shell and high resistivity to chemical reaction to inhibit alloy-shell reaction [6].

Ceramic shells are usually made from ingredients, namely the refractory filler, binder, additives and stucco material [7]. The binders used for making the ceramic shells significantly affect the quality of the produced shell. Usually, the binders are of two types, one is alcohol-based and the other is water-based. Previously, ethyl silicate which is an alcohol-based binder was mostly used in the IC industries because it hardens very quickly and provides adequate mechanical strength to the ceramic shell. However, its use had been deserted in many countries due to its toxic nature which subsequently led to an increase in the application of water-based colloidal binders in the ceramic slurries. Colloidal silica based ceramic shells are extremely brittle and highly prone to cracking mechanism.

It was investigated by Jones [8] that the ceramic moulds created by the colloidal silica binders lacks adequate unfired strength and that causes shell fracture during dewaxing process. As both wax and shell expands on dewaxing, the weak shell, unable to resist the pressure, cracks. In order to increase the shell's green strength, Harun et al. [9] added treated rice husk fibre into the ceramic slurries and it was found that the shell's green strength increased. Kline et al. [10] added graphite particles to fused silica-colloidal silica based slurry for improving the mould permeability. It was found that the permeability of the shell increased whereas the flexural strength decreased. The formation of spherical pores was modelled by Monte Carlo Simulation. The experimental data was compared with the theoretical model and finally, the addition of graphite particles in the ceramic slurries was recommended.

Everhart et al. [11] investigated the properties of the colloidal silica based ceramic shell at sharp corners and edge regions. The porosity effect on stress concentration at sharp corners of the ceramic shell was evaluated. A generalized equation was also formulated on the basis of experimental results and finite element modelling to predict the stress required to generate crack in the shell. Yahaya et al. [12] modified the back-up stucco by mixing activated charcoal to it whose percent varied from 0% to 30%. The microwave dewaxing method was employed to remove the waxes from the shells and then the green shells were fired. The authors found that percent increase in content of activated charcoal decreased the time to dewax the shells. The optimum amount of activated charcoal to be added to the back-up stucco was found to be 25%, beyond this limit cracks on the outer edges of the shell were observed. Further, it was found that the porosity and collapsibility of the shell increased, but its strength and density decreased.

Fei et al. [13] described the influence of particle size distribution (PSD) on the properties of ceramic shell prepared from zirconia solution for casting TiAl. The results showed that PSD exhibits important role in controlling the quality of IC ceramic shells. Cheng et al. [14] investigated the suitability of TiO_2-Al_2O_3 based face coat slurry to cast TiAl alloys. It was found that TiO_2-Al_2O_3 face coat formed a thick and hardened layer at metal-mould interface, which shows that it has fairly lower chemical inertness towards the TiAl alloys. Jin et al. [15] applied Bayesian network approach to identify which process parameter is uncontrollable in the production of ceramic mould in the IC process. It was suggested to apply industrial computerized tomography (CT) method to measure the inner mould cavity dimensions so that with more no. of data, the accuracy of the measurement would be enhanced. According to Ferreira and Mateus [16], the mechanical properties (both green and fired strength) of the IC ceramic shells cannot be ignored as they provide the shell with the capacity to resist stresses during the pattern burn out and metal casting stages. The literatures on IC ceramic shells show that continuously research is going on improving the ceramic shell properties and further research is needed to increase the desirable properties of the IC ceramic shells made from colloidal silica binder.

Naturally available products such as saw dust and coconut fibres are cheaply and easily available all over the world. Saw dust is obtained from sawing of wood and coconut fibre is obtained from the external shell of the coconut fruit. Ku et al. [17] found that sawdust could be successfully used as filler material for improving the mechanical properties of the polymer matrix composites. Kumaoka [18] successfully created porous ceramic using sawdust. Coconut fibres have been successfully used as good reinforcement material to improve the properties of the thermosetting and thermoplastic composite materials [19–21]. Coconut fibres and saw dust have never been used as additives in the secondary coatings of the IC ceramic shells. Thus, in the present work, influence of coconut fibres and saw dust individually into the colloidal silica shell systems has been investigated. Important shell properties such as thickness, flexural strength (green and fired), porosity and permeability of both saw dust and coconut fibre modified shells were compared with that of the conventional ceramic shell containing liquid polymer to check whether these material additions are beneficial or not. Further, the tensile strength and porosity of aluminium-silicon (Al-7%Si) alloy castings obtained from these shells were determined to check the quality of castings in each case.

2 Materials and methods

2.1 Sample preparation

Brown coconut fibres obtained from the rear end of the coconuts were extracted from the matured coconuts and soaked in water for 1–2 days to get rid of dust and other waste matter embedded along with it. Then, the fibres were sundried for

2 days to ensure that the fibres were devoid of absorbed water. Subsequently, the fibres of about 1 to 2 mm in length were cut manually. The sawdust collected from the carpentry shop was made to pass through sieve shaker to get fine particles.

2.2 Ceramic shell manufacture

Ceramic shells containing conventional liquid polymer, coconut fibre and saw dust are referred as P-type, C-type and S-type ceramic shells, respectively. The details of the ingredients used to construct the shells are listed in Table 1. The percentage of liquid polymer added to the primary slurry was 5% by weight of the slurry. However, liquid polymer, saw dust and coconut fibre additions to the secondary slurries were made at 2%, 3%, 4%, 5% and 6% by weight of the slurry. The stuccos were applied manually by rainfall sanding method. The primary coat was dried for 24 h and each secondary coat was dried for 4 h. The dewaxing of ceramic shells was done in a microwave oven at a temperature of 275 °C and later, the shells were fired at 700 °C. The prepared ceramic shells are shown in Fig. 1.

2.3 Material characterizations

The morphology of the shell was analysed by field emission-scanning electron microscopy (FE-SEM) supplied with energy dispersive X-Ray (EDX) analysis using QUANTA 200 FEG. The thermal analysis was executed using thermo-gravimetric analyser (EXSTAR TG/DTA 6300) at a heating rate of 10 °C/min from 30 °C to 600 °C temperature in presence of air. The ASTM standard methods D2395-07a [22] and E1755–01 [23] were used to determine the density and ash content of the coconut fibre and saw dust. Their apparent porosity was calculated based on the method employed by Horisawa et al. [24].

2.4 Measurement of slurry rheology

Slurry rheology influences the quality, stability and life of the slurry and it includes viscosity, density, pH value, and plate weight. The slurry viscosity was measured by means of a Brookfield DV-II + Pro Viscometer. The mass and volume method was used to determine the slurry density. pH was measured using an electronic pH meter. Plate weight (P) of the slurry was measured as per by Sidhu et al. [25].

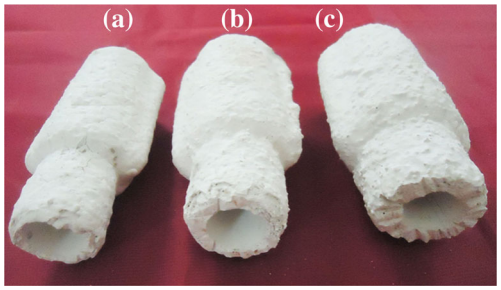

Fig. 1 Different types of ceramic shells (a) P-type (b) S-type (c) C-type

2.5 Measurement of material properties

Porosity is the amount of air space in an object and the apparent porosity (% AP) of the ceramic specimen was measured using Archimedes buoyancy technique with dry weight, soaked weight and immersed weight in water as per ASTM C20 [26] and it is given by Eq. 1.

$$\text{Apparent porosity of the ceramic shell (\%AP)} = \frac{(\text{Soaked weight} - \text{Dry weight})}{(\text{Soaked weight} - \text{Suspended weight})} \times 100 \quad (1)$$

Permeability is the ability of liquid or gas to pass through an object. The permeability of the ceramic shells was measured at 900 °C using a permeability tester. The air flow rate (F) inside the ceramic shell was altered every time and the resultant pressure drop ($\Delta P = P_1 - P_0$) was determined. The permeability (k) of the ceramic shell is given by Eq. 2 [27].

$$\text{Permeability (k) of the ceramic shell} = \frac{\mu(r_o - r_i)}{m(4\pi r_o r_i)} \quad (2)$$

where, μ is the dynamic viscosity of air, r_i *and* r_o are the inner radius and outer radius of the ceramic shell, P_i and P_o are the

Table 1 Slurry specification for building different ceramic shells

Slurry composition for different layers in each shell						P-type shell	C-type shell	S-type shell
Coating	Binder	Antifoam	Wetting agent	Filler	Stucco	Additive	Additive	Additive
Primary	NCS	Yes	Yes	Zircon	Zircon sand (−200)	Liquid polymer	Liquid polymer	Liquid polymer
Sec-1	NCS	No	No	AS	Molochite (30/60)	Liquid polymer	Coconut fibre	Saw dust
Sec-2	NCS	No	No	AS	Molochite (16/30)	Liquid polymer	Coconut fibre	Saw dust
Sec-3	NCS	No	No	AS	Molochite (16/30)	Liquid polymer	Coconut fibre	Saw dust
Seal	NCS	No	No	AS	-	Liquid polymer	Coconut fibre	Saw dust

Sec = Secondary layer, NCS = Nano-based colloidal silica, AS = Alumino-silicate, P-type = Conventional shell, C-type shell = Coconut fibre modified shell, S-type shell = Saw dust modified shell

inner and outer pressures of shell sample and m is the slope of the regression curve plotted between ΔP and F.

Flexural strength or modulus of rupture (MOR) was carried out for both green and fired ceramic shells over a span length of 50 mm at an ambient temperature of 22 °C on a UTM machine. The flexural strength, σ_{Max} is given by Eq. 3 [28].

$$\text{Flexural strength } (\sigma_{Max}) = \frac{3P_{Max}l}{BH^2} \quad (3)$$

where, P_{Max} is the fracture load (N), l is the span length, B is the width of the shell (mm) and H is the shell thickness (mm).

The apparent porosity of the casting was measured by weight loss method as given by Eq. 4. The hypoeutectic Al-Si alloy was used for casting inside ceramic shells and its theoretical density is 2.68 g/cm^3.

$$\%AP_{cast} = \frac{(\text{Theoretical alloy density} - \text{Actual casting density})}{\text{Theoretical alloy density}} \times 100 \quad (4)$$

3 Results and discussions

3.1 Materials characterization

The physical properties of additives namely, conventional liquid polymer, coconut fibre and sawdust are presented in Table 2. Porosity tests revealed that both saw dust and coconut fibres are more porous than the liquid polymer. The microstructural images of saw dust and coconut fibre at high magnification is shown in Fig. 2 and it is found that both additives inherently possess porous morphology. This porous structure of the additives is helpful for superior interlocking between the additives and the ceramic matrix. Further, it is noticed that the liquid polymer was denser than the saw dust and coconut fibres and that of saw dust was lowest. As the porosity of saw dust was more than that of coconut fibre, therefore the density of saw dust was less compared to coconut fibres, which shows that more amount of saw dust can be added for equal weight percentage of the slurry.

It is found that the ash content of liquid polymer is negligible because of which it was added to the primary layer in all shells. However, the ash content of the coconut fibre was found to be more than that of the saw dust. The additives namely, sawdust and coconut fibres are wood products. Natural wood products cannot be free from ash and so only they were added to the secondary slurries in the present study. They contain cellulose, lignin and water. The cellulose and lignin are tightly bound together. DTA analysis of both saw dust and coconut fibres was done to determine their thermal stability and burning temperatures (Fig. 3). It was found that the burning temperature of saw dust was 387 °C and the same for coconut fibre was about 432 °C, though burning began at 297 °C, which coincided with its decomposition temperature. It is essential that the shell dewaxing temperature should be less than the additive burning temperatures to increase the shell's green strength and thus, the dewaxing temperature of 275 °C has been chosen in the present analysis. The additives remain inside the ceramic shell after the dewaxing process and it also contains many impurities such as dust, absorbed traces of wax, etc. besides additives.

Table 2 Physical properties of additives used in the ceramic slurry

Physical properties	Liquid polymer	Coconut fibre	Saw dust
Density (g/cm^3)	1.05	0.61	0.22 g/cm^3
Ash content (%)	Nil	2.98	2.52
Porosity (%)	40	60	76

The colour of the dewaxed shell (Also known as green shell) is pale yellowish in colour as shown in Fig. 4. In the present study, the ceramic shells were fired at 700 °C for 4 h. Carbonization is the conversion of organic substance into carbon. The carbon residues in the form of ashes are formed at temperatures about 300 °C. If these ashes remain in the ceramic shell, then there is a greater possibility of reaction of ash with the molten material which will degrade the mechanical properties of the casting. However, when the shells are fired at high temperatures, these ashes and other impurities which remained in the shell after dewaxing are removed. It has been found that both gas and electric ovens lack sufficient oxygen if insufficient care is taken in the operational procedures. Around 8–10% free oxygen should ideally be present for residue removal [1]. Electric ovens should have provisions for free through-flow of air by efficient venting. Therefore, in the present study, open-top muffle furnace has been used to fire the ceramic shells and it was found that the fired shells were super white in colour devoid of any impurities (Fig. 1).

3.2 Slurry rheology

The slurry properties for all ceramic shells are stated in Table 3.

It is found that the primary slurry had higher density, viscosity and plate weight than the secondary slurries containing polymer, coconut fibres and saw dust which is also advantageous. The reason behind is that the particle size of the zircon flour used as refractory material in constructing the primary or first layer is smaller in size than that of the Alumino-Silicate flour used in secondary layers. The size of zircon flour is −325 mesh whereas that of Alumino-Silicate is −200 mesh (Fig. 5) and the fine morphology of the zircon flour is essential to provide a smooth surface finish to the internal surface of the

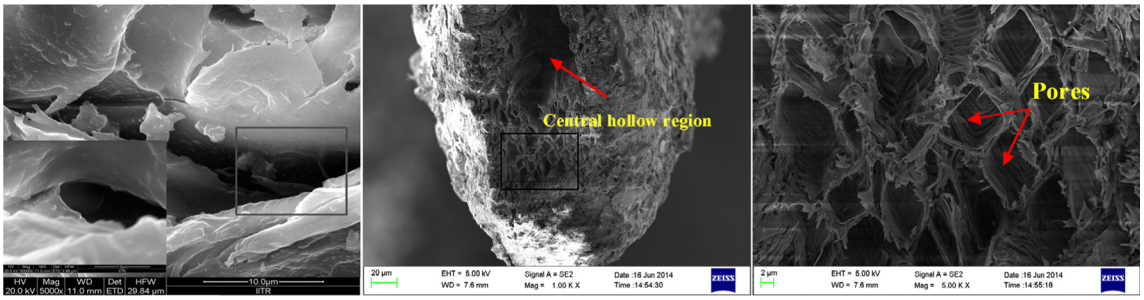

Fig. 2 Cross-sectional view of (a) Saw dust showing pore (b) Coconut fibre showing central hollow region & honey-comb like pores

ceramic mould. The primary slurry with low viscosity/ density/ plate weight would cause the stucco material to penetrate into the primary layer thereby decreasing the surface texture of the inner mould, as shown in Fig. 6 (a). If the primary slurry is too viscous, it would lead to uneven draining, thereby producing a localized thick coating, which might part away during dewaxing or casting due to insufficient adhesion between the primary and back-up layers, as shown in Fig. 6 (b).

It is found that the density, viscosity and plate weight of the coconut fibre-modified secondary slurry were more than that of other two slurries for equal weight percentage of additives. The slurry density and viscosity of liquid polymer modified slurry at 6 wt% is less than that of other two slurries at 4 wt%. Ceramic retention verses drain time for all the three slurries have been plotted as shown in Fig. 7. It is seen from the graph that the coconut fibre-modified secondary slurry had highest ceramic retention rate and reduced drain time as compared to other two slurries. Water holding capacity is defined as the quantity of water that is bound to the fibres without the application of any external force except for gravity and atmospheric pressure. It has been found that coconut fibres have very high water holding capacity [29] as it can hold water within the bees-web like pores present inside it and also, it can retain water in the outer fibrous structure. The shape and size of central hollow cavity inside the coconut fibre depends on the thickness of the cell wall and the source of the fibre. So, the coconut fibres in the secondary ceramic slurry would have absorbed more amount of water from the slurry and thus, made the slurry more dense and viscous as compared to other two slurries. However, the properties of the slurry as well as of the ceramic shell will change, if the size of coconut fibres is varied. In the present study, the size of the coconut fibre has been considered as a fixed parameter to simplify the study to test its viability for building the ceramic shells for investment casting. On the other hand, the author is committed to perform a future study to analyse the variability of the coconut fibres in influencing the properties of the ceramic shell. The pH of all slurries lied in between 9.3 to 9.5 and there was no gelling of the slurries, which shows that the pH of slurries was satisfactory.

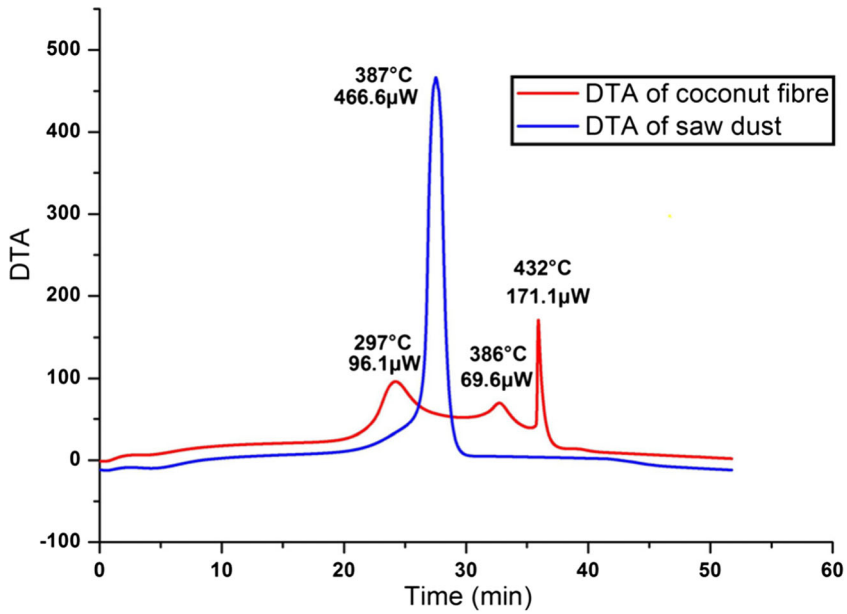

Fig. 3 DTA curves of saw dust and coconut fibre

Fig. 4 Ceramic shell absorbed wax from wax pattern during dewaxing

3.3 Shell thickness

In IC process, immersing, stuccoing and drying sequence of ceramic layer over the disposable pattern is repeated until the required thickness of the shell is attained. The variability of shell thickness influences the ability of the shell to absorb heat from the melt and its ability to expand on heating. Heat transfer rate is reduced in thicker shells, on the other hand, its strength increases. Thicker shells expand less on heating and are capable of resisting contraction on cooling. However, thinner shells are very weak and fragile, and cracks easily. Usually, the shell build at the corners are different from that at regular flat section, due to position of the stucco and additive particles. The disparity of the structure in these regions of the shell causes it to break under smaller loads.

In Fig. 8(a) and (b), thicknesses of ceramic shells with different weight percentage of additives at regular section and sharp corners have been plotted. It is found from Fig. 8 that the shell thicknesses of C-type and S-type ceramic shells are overall 23.27% and 14.78% more than the P-type ceramic shell for a five-layered shell system at regular section. However, the C-type ceramic shell was 7.4% more thick than the S-type ceramic shell. Similarly, C-type and S-type ceramic shells showed 44.9% and 34.2% more thickness from that of P-type ceramic shell at sharp corners. The C-type ceramic shell was 8% thicker than the S-type ceramic shell.

The shell thickness is directly influenced by the slurry density, viscosity, ceramic retention rate and stucco particles. Here the size of stucco was same for all cases. The more the aforementioned slurry properties, the more thick shell will be formed. The thickness of the C-type ceramic shell was found to be highest among all shells because the coconut fibre-modified ceramic slurry possessed comparatively higher density, viscosity and ceramic retention rate than the other two slurries. On the other hand, thickness of S-type ceramic shell was also appreciable as regards to conventional ceramic shell.

3.4 Shell porosity

In investment casting industries, the porosity in the shells is initiated through sacrificial additions of costly liquid polymer and nylon fibres, graphite particles, etc., to lower the thermal diffusivity. The discrepancy in levels of porosity strongly influences the mechanical and thermal properties of ceramic shells. Owing to wide variety of shell compositions, particle size distribution, and processing parameters, the ceramic shell could have from (10) to 30 % porosity, which can provide air or steam permeability [30]. It is essential for the ceramic shell to have moderate porosity with some fraction of inter-connected porosity to provide permeability. Otherwise, the gases will finally remain in the aluminium alloy castings in the form of gas porosity, leading to inferior mechanical properties.

The apparent porosity of the three different fired ceramic shells obtained from different weight percentage of additives is plotted in Fig. 9. It is found from the graph that the porosity

Table 3 Characteristics of the ceramic slurries for ceramic shells

Properties	Primary slurry	Additive Weight %	P-type slurry	C-type slurry	S-type slurry
			Secondary Slurry		
Density (gm/cm^3)	3.049	2	1.347	1.411	1.392
		3	1.369	1.522	1.436
		4	1.398	1.673	1.505
		5	1.423	1.748	1.579
		6	1.452	2.316	1.967
Viscosity (cp)	1840	2	986	1084	1039
		3	1038	1137	1115
		4	1071	1282	1192
		5	1132	1425	1228
		6	1158	1501	1345
Plate weight (g/cm^2)	0.179	2	0.164	0.191	0.182
		3	0.176	0.206	0.195
		4	0.183	0.219	0.208
		5	0.191	0.234	0.225
		6	0.201	0.248	0.236

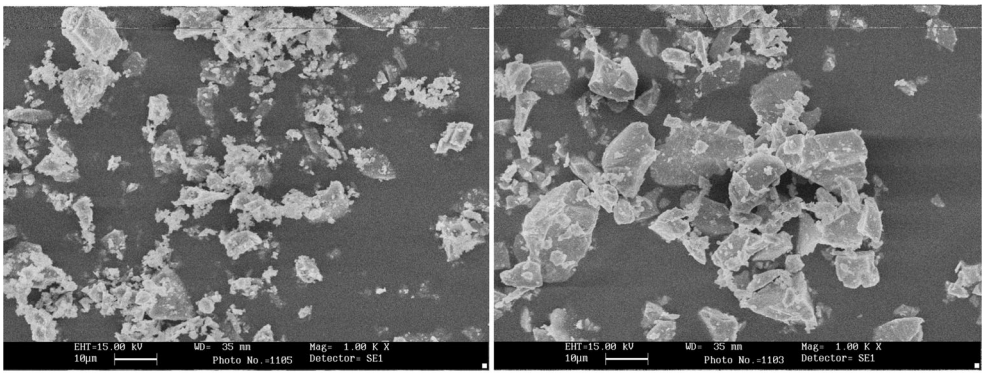

Fig. 5 SEM micrographs of refractory fillers (a) Zircon flour (b) Aluminium silicate

of P-type shell is lowest, whereas S-type shell exhibited maximum porosity at the same percentage of additive content. It is due to the fact that sawdust possessed least density among all additives. So, more no. of saw dust particles was embedded in the ceramic shell which caused more number of pores on shell firing. It is followed by C-type ceramic shell since the density of coconut fibres is less than the liquid polymer. The same phenomenon occurred in this case and shell's porosity increased. Figure 10 shows the pores created on burning out of liquid polymer, saw dust and coconut fibres and it is evident that the pore size created due to burn out of saw dust particle is maximum which increased the porosity of the S-type shell significantly. It can be said that the porosity depends on shell building process parameters such as type and quantity of additives, slurry characteristics and stucco size (constant parameter in this case). As the percentage of additives within the shell increased, the percentage of resulting pores that were open to the surfaces also increased.

3.5 Shell's hot permeability

The permeability of the shell is of high importance to the IC industries. The shell must be capable of allowing gases to pass through with atleast the same rate as melt enters the shell. If gases cannot exit the shell faster than it is filled, then air pressure increases within the shell. This build up of pressure can result in incomplete shell filling, shell cracking and gas defects in castings. Mostly, the IC shells are impermeable and the main reason is the use of fine particle-size material with high packing density in shell construction. While the dense structure gives high strength at low thicknesses, it restricts the flow of gases. Thus, pore-formers namely, liquid polymer, coconut fibres and saw dust have been added in the present study for see their impact on shell's permeability.

The permeability values of different shells at different weight percentage of additives were determined using Eq. 2 and shown in Fig. 11. It is clear from the figure that the hot permeability of S-type shell is more than P-type and C-type ceramic shells by 19.85% and 7.1%. The permeability of the IC shell mould depends on its percent porosity. The more porous the ceramic shell, more easily the hot gases will escape out of shell. As the S-type shell was the most porous one among the three types of constructed shells, therefore, its hot permeability value was also the highest and thus, the hot air generated due to heated melt can be expelled quickly from the shell.

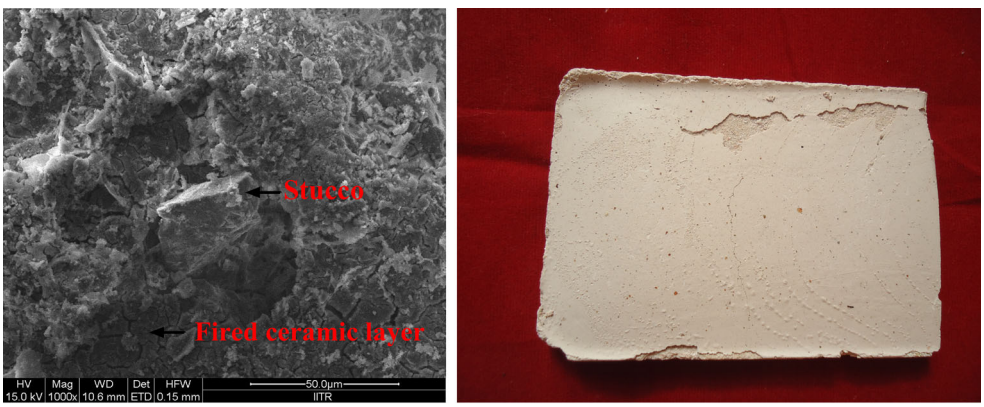

Fig. 6 Primary layer depicting (a) Stucco penetration (b) A portion being parted away

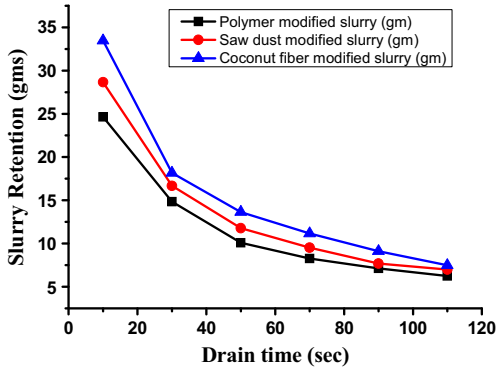

Fig. 7 Graph showing drain time verses slurry retention for different slurries

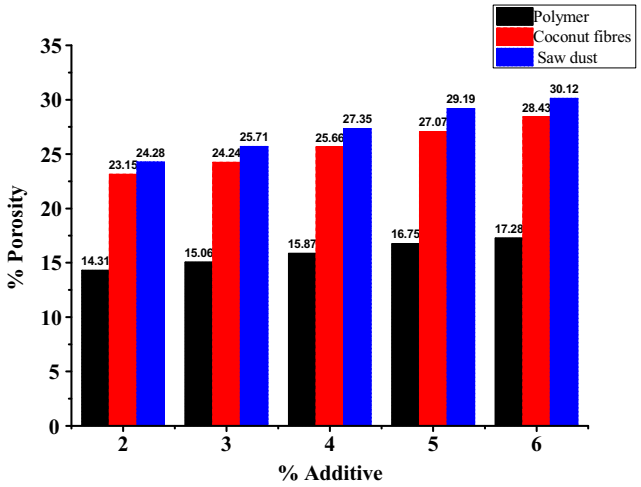

Fig. 9 Apparent porosity of different types of shells

3.6 Shell flexural strength

The flexural strength of different ceramic shells at different weight percentage of additives at both green and fired states was determined using Eq. 3 and shown in Fig. 12. The green strength of C-type shell is found to be maximum which is followed by S-type shell, while P-type shell showed least strength which is well in agreement with Jones [8] as polymer modified shells lack sufficient green strength leading to shell cracking during dewaxing. It is seen that the green flexural strength of both C-type and S-type shells increase with percent increase of additives up to 5 weight percentage. Beyond this limit, the green strength decreases which indicate that this is the optimum limit for adding additives in the ceramic slurry.

The morphology of saw dust [31] and coconut fibre is shown in Figs. 13 and 14. It is apparent that the surface of both particles is very fibrous in nature. At higher magnification (Fig. 13 b), it is observed that the fibrous surface of the saw dust particle contains many irregular scales and these scales are attached to one another in such a way that a small trough is formed at irregular spaces. The SEM micrograph of the coconut fibre reveals many irregular un-detachable flakes (Fig. 14 (a, b)). The morphology of these flakes at much higher magnification shows that the flakes are joined by web like structure (Fig. 14 (c)).

Both saw dust and coconut fibres are hydrophilic in nature and because of which the ceramic slurry is entrapped in between the trough or webs formed by these natural additives, thereby making the bond extra strong (Fig. 15). However, C-type ceramic shell showed more strength than the S-type ceramic shell because there is comparatively better alignment of the coconut fibre in the ceramic matrix which increased the flexural strength of the C-type ceramic shell [32]. Further, it was found by Li et al. [33] that the tensile strength of the coconut fibres is very high i.e. (142 ± 36) MPa, as it contains highest percentage by volume of lignin, which makes the fibre very tough and stiffer as compared to other natural fibres. When it is embedded in the ceramic matrix, the adhesive force between the flakes of the coconut fibre and the ceramic material is so strong that it is very difficult to pull out from the ceramic matrix. Further, the bond between the saw dust/coconut fibre and ceramic matrix can only be formed if they do not get burnt during dewaxing of the ceramic shell and

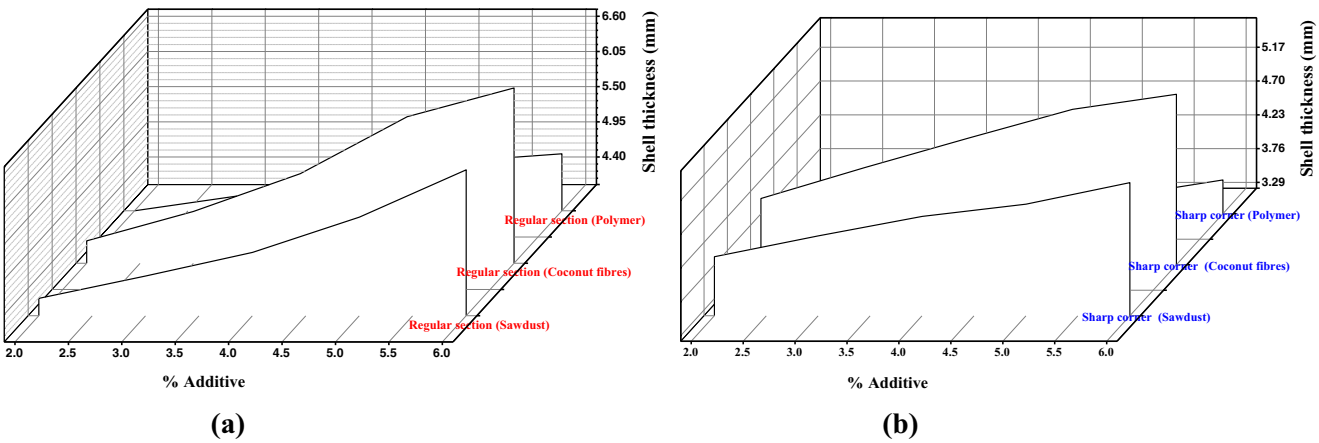

Fig. 8 Shell thickness at different percentage of additives at (a) Regular section (b) Sharp corner

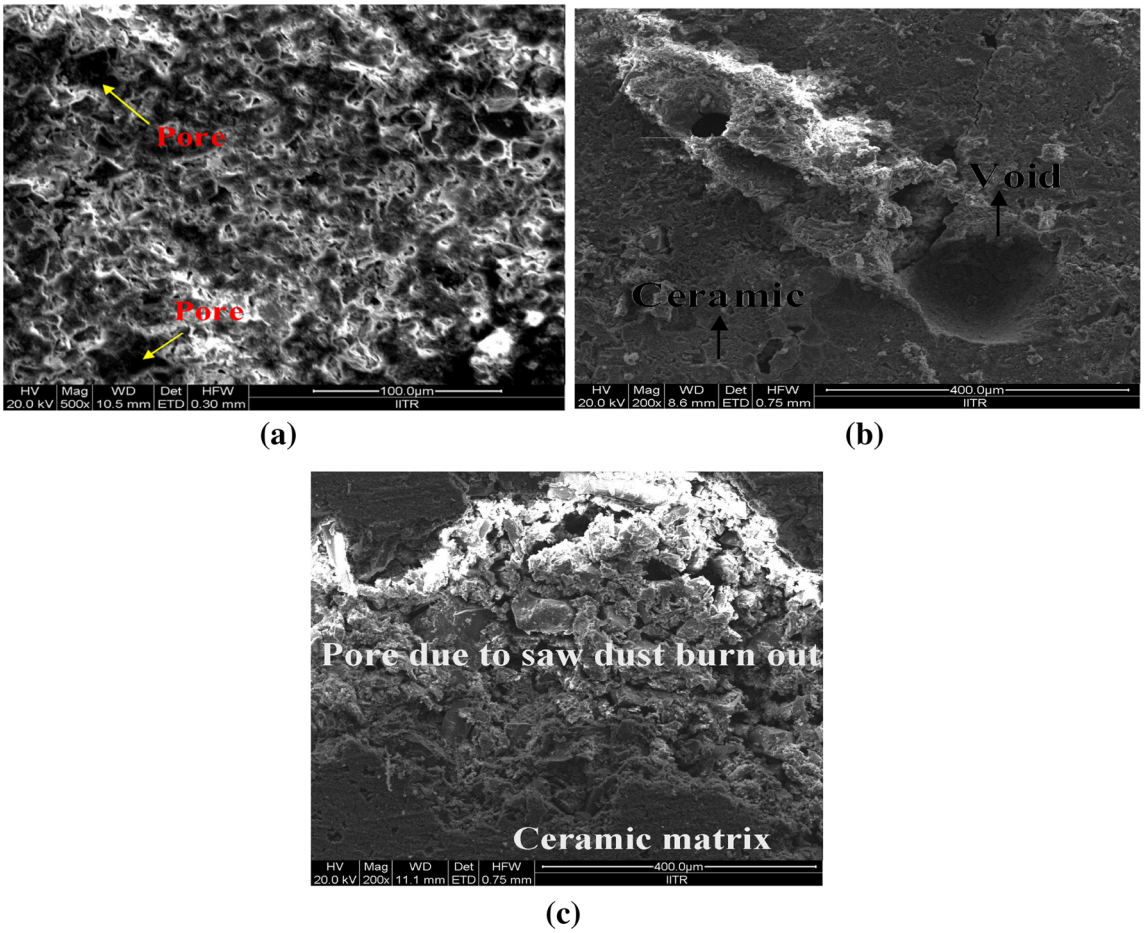

Fig. 10 Pores formed after shell firing in place of (a) Liquid polymer (b) Coconut fibre (c) Saw

remain intact within the matrix. It is only possible if the dewaxing temperature is lower than the additive's burning temperatures. However, there is always an optimum limit to the additive addition in the ceramic slurry. If excess quantity of these particles is reinforced, then the additive distribution is not uniform in the slurry and cluster of these particles accommodate in a single space with very poor bonding with the ceramic matrix, thereby decreasing the strength.

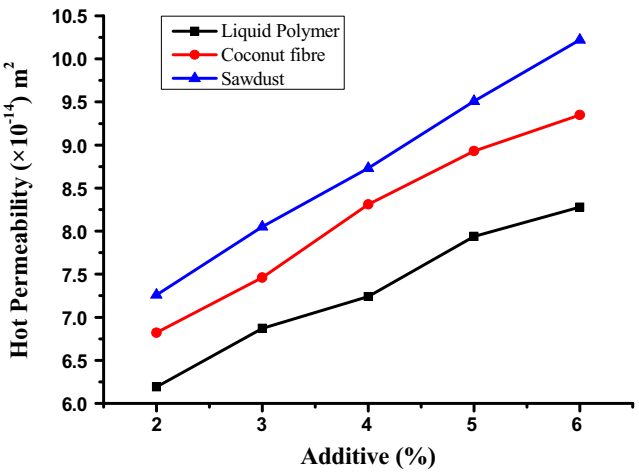

Fig. 11 Hot permeability of different ceramic shells

The fired strength of the ceramic shells showed a decreasing trend in all cases and it was found to be highest for C-type shell. The fired strength of the ceramic shell depends on shell's thickness and its porosity content. The C-type shell was thickest among all shells with adequate porosity and sintering further increased its strength. Hence, it possessed higher fired strength as compared to other shells. A ceramic shell should have sufficient fired strength to bear the heat and weight of the molten alloy. However, excessive fired strength would create difficulty in breaking the shell to remove the casting from it. Many research works had been carried out in the past to reduce the fired strength of the ceramic shells. In this investigation, fired strength has been automatically reduced besides increase of other favourable properties such as porosity and permeability of the shell.

3.7 Shell cracking

Shell cracking is partly due to the shell properties specially, strength and permeability, and partly due to the dewaxing process. Actually, there is a considerable difference between the

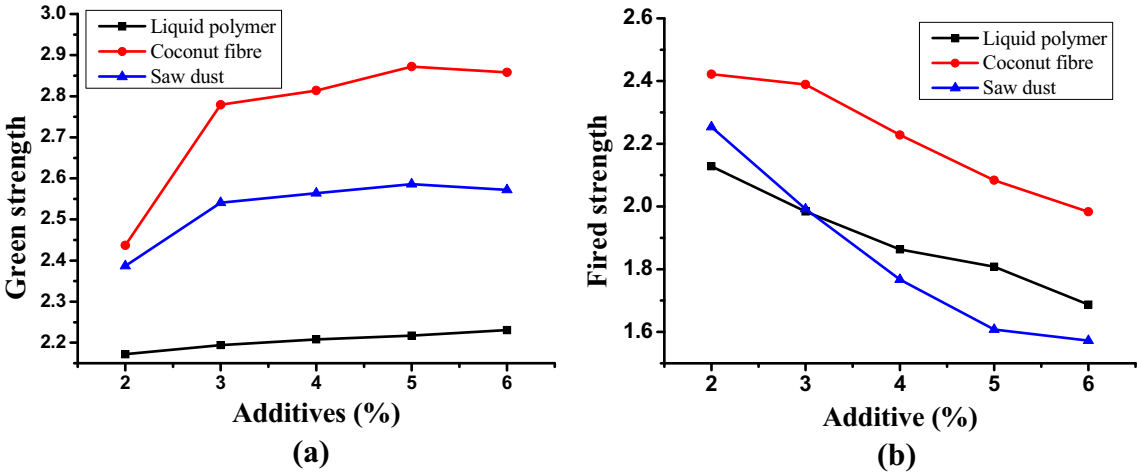

Fig. 12 Flexural strength of different ceramic shells at different weight % age of additives (a) Green strength (b) Fired strength

Fig. 13 Morphology of saw dust at (a) Low magnification

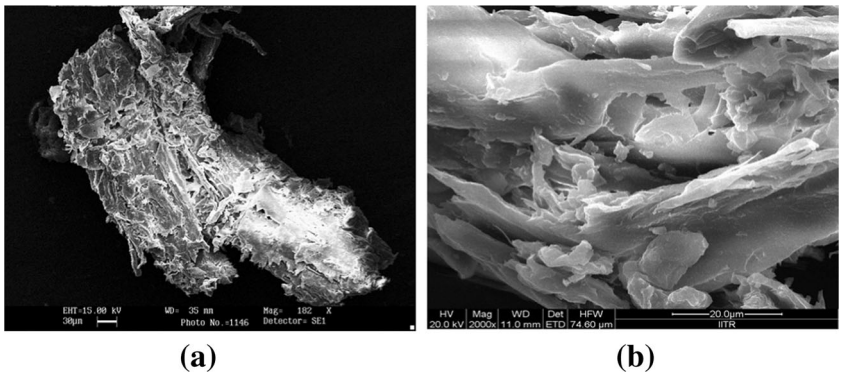

Fig. 14 Morphology of (a) Coconut fibre containing flakes (b) Flakes at higher magnification (c) Flakes joined by webs

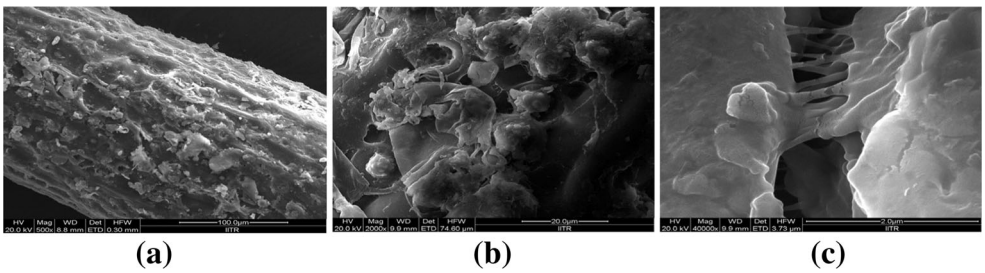

Fig. 15 Microstructure in ceramic matrix (a) Embedded saw dust (b) Longitudinal view of the embedded coconut fibre (c) Top view of the embedded coconut fibre

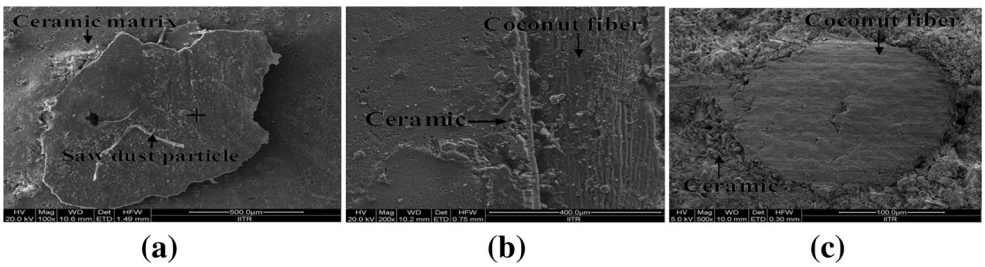

Table 4 Visual inspection of shell cracking in different ceramic shells

Shell	Additive	Weight Percent (%)	Inspection
P-type	Liquid polymer	2	Fracture
		3	No fracture
		4	No fracture
		5	No fracture
		6	No fracture
C-type	Coconut fibre	2	No fracture
		3	No fracture
		4	No fracture
		5	No fracture
		6	Fracture
S-type	Saw dust	2	No fracture
		3	No fracture
		4	No fracture
		5	No fracture
		6	Fracture

low thermal expansion of the ceramic materials and the high thermal expansion of the waxes. The expanding wax stresses the ceramic shell and if the intensity of the generated thermal stress is more than the shell's strength, the shell cracks. This cracking phenomenon in shells usually develops along the path of least resistance to lessen the stress caused by volumetric expansion of waxes. The occurrence of cracks in the ceramic shells can be reduced if the generated stresses are reduced.

Generally, a ceramic shell can relieve the stress through three mechanisms: (1) Reducing the expansion of the wax during melting, (2) Increasing the shell's strength, (3) Increasing the shell's permeability. Till date, a lot of research works on reducing expansion rate of investment casting waxes have been patented and these waxes are available for commercial applications. Moreover, the wax patterns should be gated to the central sprue in such a way that the drainage of molten wax takes place rapidly and easily. The shell's strength can be increased if more number of ceramic layers is built over the wax pattern and very fine refractory fillers are used, but it decreases the permeability of the shell which is not desirable as it increases the shell cracking intensity. If the shell is adequately permeable, the molten wax penetrates quickly into

Fig. 16 Cracked shell due to increased percent of additives

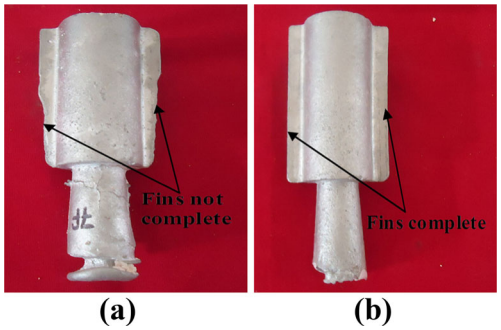

Fig. 17 (a) Defective investment casting (b) Complete investment casting

the shell through the pores thus reducing pressure on the shell and ultimately, shell cracking is reduced. There is always an optimum value of additives that should be added to the secondary layers to get a crack free ceramic shell during dewaxing. However, there is another important consideration is the viscosity of the wax. Highly viscous wax should not be used for preparing wax patterns as it would make the penetration of molten wax into the ceramic shell more difficult.

Table 4 presents the visual inspection of shell cracking in different ceramic shells with different percentages of additives. It can be seen that P-type shell cracked at 2% liquid polymer content. It happened because the shell was very weak and thin, and least impervious so that it was unable to bear the pressure of expanding wax during dewaxing process and it cracked. Porous ceramic shell provides space to the expanding wax thereby relieving the stress on ceramic shell and thus, shell cracking is reduced. However, too porous shell also causes shell cracking, as it happened in case of 6 wt% additions of coconut fibres and saw dust to the ceramic slurries (Fig. 16). It is due to the fact that more amount of uneven loading of additives in the ceramic matrix with more porous structure led to shell cracking at 6 wt% addition in case of both C-type and S-type ceramic shells.

3.8 Effect of shell porosity on casting

The most common IC defects which arise due to poor shell permeability or porosity are mis-run i.e. the molten alloy could not fill the ceramic shell completely leading to imperfect casting and increase of porosity in the cast parts. Figure 17 shows the images of both defective and complete investment

Table 5 Effect of casting porosity on tensile strength

Shell	Mean Tensile strength (MPa)	Mean Casting porosity (%)
P-type	104.3	3.26
C-type	119.2	2.41
S-type	121.0	2.17

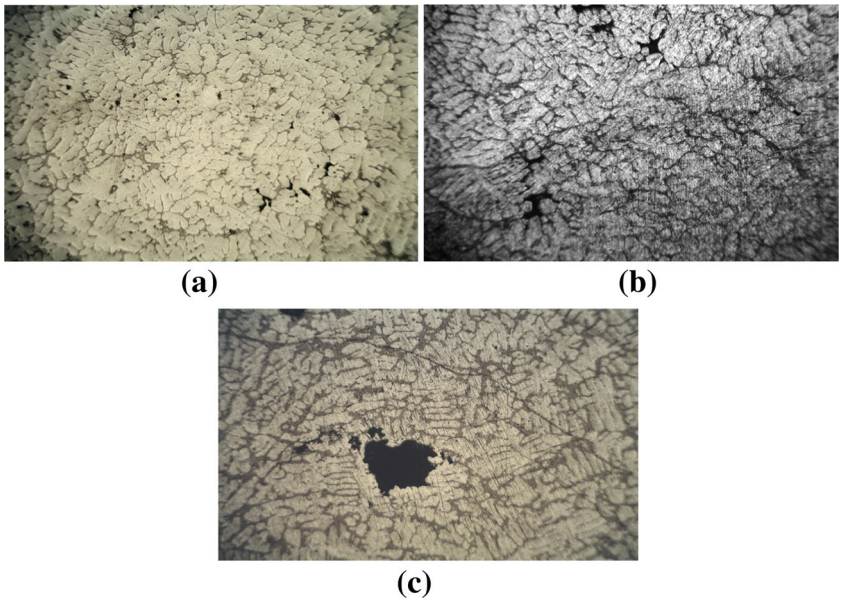

Fig. 18 Microstructures of Al-7%Si alloy casting at magnification 50X casted in different ceramic shells (a) S-type shell (b) C-type shell (c) P-type shell

castings. It is clear that the fins provided at the ends of the casting are very thin i.e. 5 mm width and 2 mm thickness. The only problem that occurred to cast this structure was the partial filing of the shell due to entrapment of air around the fins. The first casting (defective one) was cast in a less permeable and porous P-type ceramic shell, while the second casting was cast in a highly permeable and porous S-type ceramic shell and its superiority over its counterpart is apparent from the figure itself.

Al-7%Si alloy investment castings were obtained from P-type, C-type and S-type ceramic shells containing 5% additive and the obtained cast parts underwent tensile strength and porosity tests. The results are shown in Table 5. It is seen that the tensile strength is highest for the casting obtained from S-type ceramic shell showing least apparent porosity, whereas the same is lowest for P-type ceramic shell showing most apparent porosity. It occurred due to the fact that the former shell being very permeable allowed the hot gases of the melt to

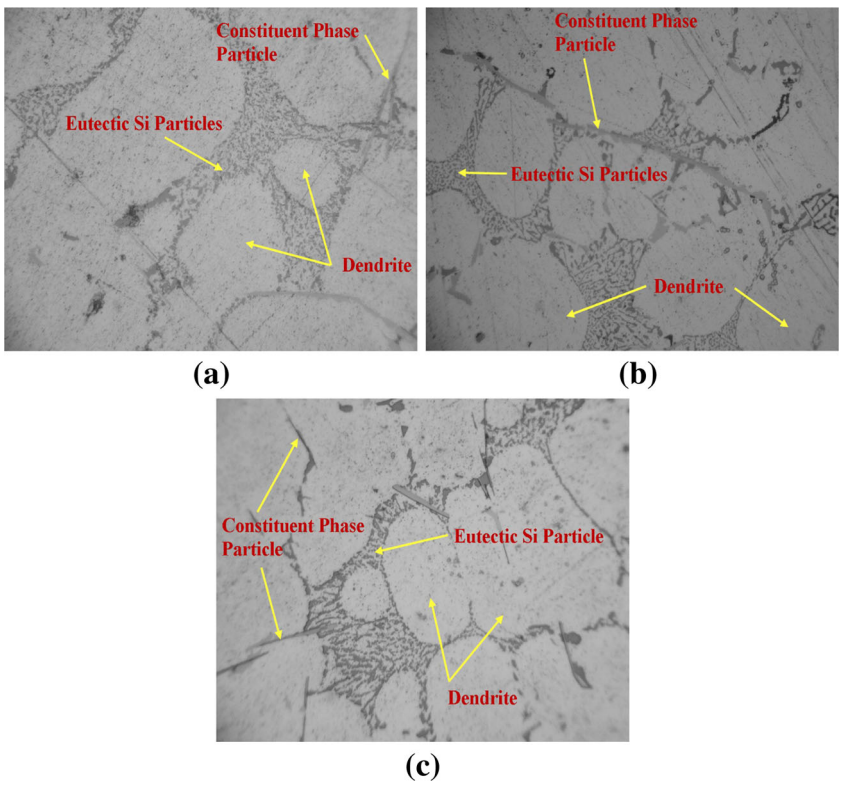

Fig. 19 Microstructures of Al-7%Si alloy casting at magnification 500X casted in different ceramic shells (a) S-type shell (b) C-type shell (c) P-type shell

Table 6 Statistical analysis of the results obtained for different slurry properties

Properties		P-type slurry	C-type slurry	S-type slurry
Density (gm/cm^3)	Mean	1.3978	1.734	1.5758
	Standard error	0.01869	0.15683	0.10281
	Median	1.398	1.673	1.505
	Standard deviation	0.04178	0.35068	0.22988
	Sample variance	0.001745	0.122979	0.052847
	Range	0.105	0.905	0.575
	Minimum	1.347	1.411	1.392
	Maximum	1.452	2.316	1.967
	Confidence level (0.95%)	0.05188	0.4354	0.2854
Viscosity (cp)	Mean	1077	1285.8	1183.8
	Standard error	31.16408	80.17692	51.82026
	Median	1071	1282	1192
	Standard deviation	69.68500	179.28106	115.87363
	Sample variance	4856	32,141.7	13,426.7
	Range	172	417	306
	Minimum	986	1084	1039
	Maximum	1158	1501	1345
	Confidence level (0.95%)	86.5254	222.6068	143.8761
Plate weight (g/cm^2)	Mean	0.193	0.2196	0.209
	Standard error	0.01058	0.01004	0.00977
	Median	0.193	0.219	0.208
	Standard deviation	0.02365	0.022457	0.021856
	Sample variance	0.00056	0.000504	0.000478
	Range	0.057	0.057	0.054
	Minimum	0.164	0.191	0.182
	Maximum	0.221	0.248	0.236
	Confidence level (0.95%)	0.028	0.029	0.027

move outside the shell in a speedy manner. It was found that the cooling rate of Al-7%Si alloy casting was comparatively more in S-type ceramic shell i.e. 0.9 °C/s whereas P-type and C-type ceramic shells exhibited casting cooling rates of about 0.7 °C/s and 0.4 °C/s. The tensile strength of C-type ceramic shell was in between the P and S types of shells, but the strength was appreciable showing 14.3% increase from the P-type ceramic shell. Tensile strength of the casting is directly proportional to the cooling rate and indirectly proportional to the porosity present in it. Micro-structural investigations at 50X and 500X magnifications were done to prove the findings as shown in Figs. 18 and 19.

It is evident from Fig. 18 that the casting obtained from S-type ceramic shell (whose cooling rate is highest) comprises of abundant small pores compared to those obtained from P-type and C-type ceramic shells. The small sized pores accommodate little cross-sectional area and thus, heavier loads can be applied to the casting. With decrease in cooling rates, the size of the pores increased and reduced in quantity. In Al-Si alloy, the white region is the aluminium dendrites while the greyish black region is the eutectic silicon particles. As casting cooling rate decreases, the size of dendrites increases, thereby decreasing the strength of the cast part.

In Fig. 19, eutectic Si particles and constituent phase particles such as iron needles (AlFeSi) are seen in all cases. However, the size of these particles is bigger in the part obtained from P-type ceramic shell. At higher cooling rates (in S-type and C-type ceramic shells), these particles are smaller in size. When the cooling rate of casting is decreased, more time is available for these particles to grow in size and they become large and form needle like brittle structures which weakens the mechanical properties of casting, as in case of P-type ceramic shell.

3.9 Statistical analysis of shell properties

Higher slurry properties are desirable for forming a desired thickness quickly around the wax pattern with only few coatings. Statistical analysis of the properties of the different secondary ceramic slurries is shown in Table 6. It can be visualized that the means, medians, and standard deviations are different for each of the slurries and the experimental results

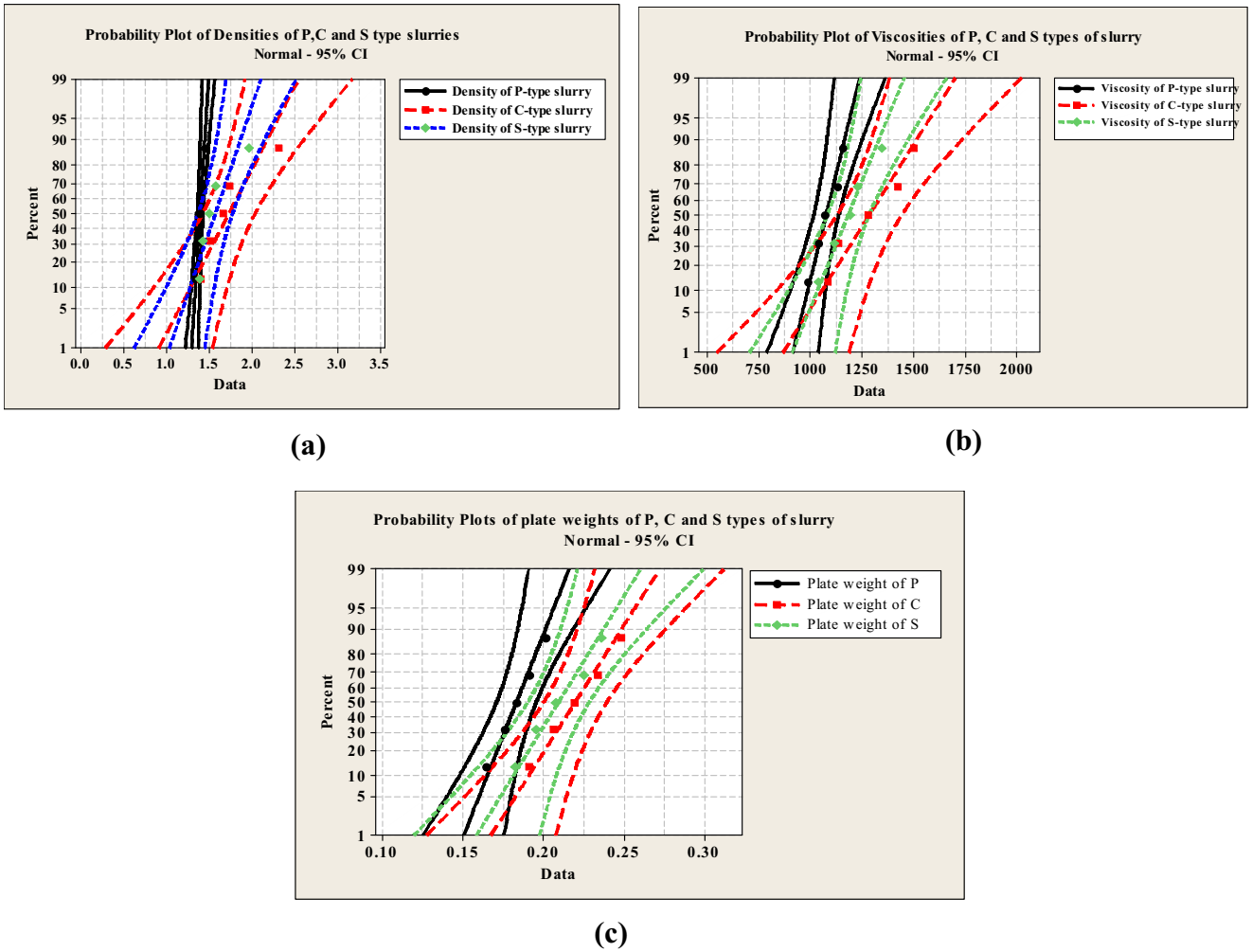

Fig. 20 Probability plots for P, C and S-types of ceramic slurry (a) Density (b) Viscosity (c) Plate weight

were found to be better for C-type slurry with more number of the data falling in 95% confidence interval. Further, probability plots of the characteristics (density, viscosity and plate weight) of different ceramic slurries have been depicted in Fig. 20 for comparing the data sets. The advantage of probability plot is that the distribution fit can be judged simply by viewing how the points fall about the line. It can be seen that the variability (spread or dispersion) of the P-type slurry is the least and that of the C-type slurry is the most among the three slurries, which indicates that the increment of percentage

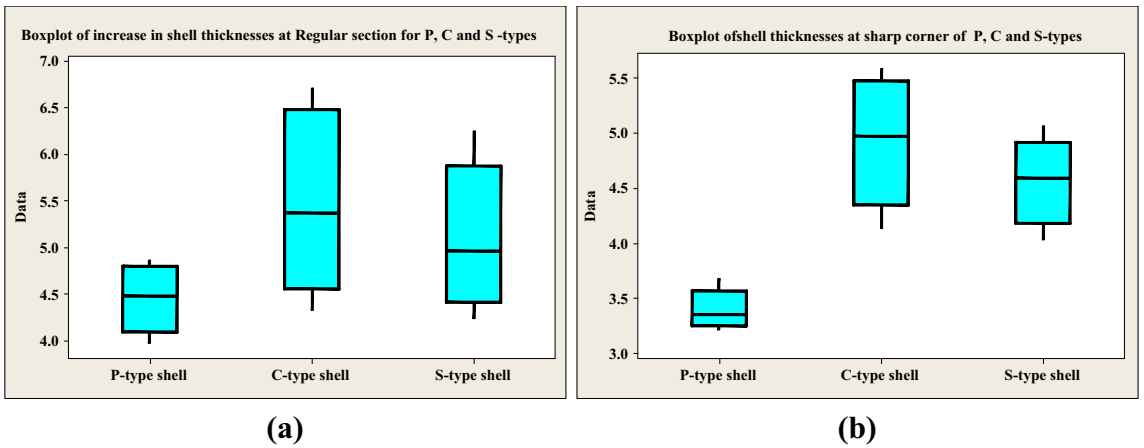

Fig. 21 Box plots of shell thicknesses for P, C and S-types at (a) Regular section (b) Sharp corner

Table 7 Box plot data of shell thicknesses of different ceramic shells

Section	Shell (mm)	P-type	C-type	S-type
Regular	Quartile Q1	4.09	4.55	4.415
	Median	4.48	5.37	4.96
	Quartile Q3	4.8	6.485	5.88
	Inter quartile range (IQR)	0.71	1.935	1.465
	Whiskers to:	3.97, 4.86	4.32, 6.71	4.24, 6.25
	N	5	5	5
Sharp corner	Quartile Q1	3.25	4.345	4.175
	Median	3.35	4.97	4.59
	Quartile Q3	3.565	5.475	4.91
	Inter quartile range (IQR)	0.315	1.13	0.735
	Whiskers to:	3.21, 3.68	4.13, 5.58	4.03, 5.06
	N	5	5	5

of coconut fibres in C-type slurry affects the slurry properties the most, which is followed by S-type slurry. Since all the points fall within the 95% confidence interval, it shows that normality assumption is acceptable.

A thicker shell provides a base to achieve an increase in the load bearing capacity of the shell. For casting complicated shapes, the shell thickness build-up ability around the disposable pattern is vital not only on flat surfaces, but more crucially around the thin and sharp edges. Due to its unique geometry, it is difficult to retain slurry and stucco sand on it. Consequently, the sharp corner becomes the weakest point and is most prone to shell cracking. Foundries build shells with extra coats just to build up sufficient thickness around the sharp corner. The extra coats typically provide little benefit to the rest of the shell.

Box plots are further plotted for the shell thicknesses at regular section and sharp corner for different shells (Fig. 21) to see the dispersion (spread) of the data. It is a proficient graphical tool for demonstrating some significant data features such as the centre, spread, departure from symmetry and identification of unusual observations or potential outliers through three quartiles (Q_1, Q_2 and Q_3) and the minimum and maximum observations (denoted by straight lines below and above the box) [34]. In a box plot, the box encloses the interquartile range (IQR), and its lower and upper bounds are the first (Q_1) and third (Q_3) quartile. Median (Q_3) is the middle value of the data set and is shown by the line that divides the box into two parts. There are two limits in a box plot, the lower limit (LL) and upper limit (UL). Any observations outside of these are called outliers. The vertical lines above and below the box are defined as the whiskers.

The box plot data for different shells for five numbers of coats are presented in Table 7. For the P-type shell, half the shell thicknesses for regular section and sharp corners are in between 4.09 mm and 4.8 mm, and 3.25 mm and 3.565 mm, whereas the same are highest for C-type shell which is followed by S-type shell. The variability of shell thickness at both sections is highest for C-type shell. From Fig. 21 (b), it is found that the distribution is negatively skewed at sharp corners for both C and S type of shells, which indicate that the data constitute higher frequency of low valued scores. No outliers are found in both cases for the different shells and

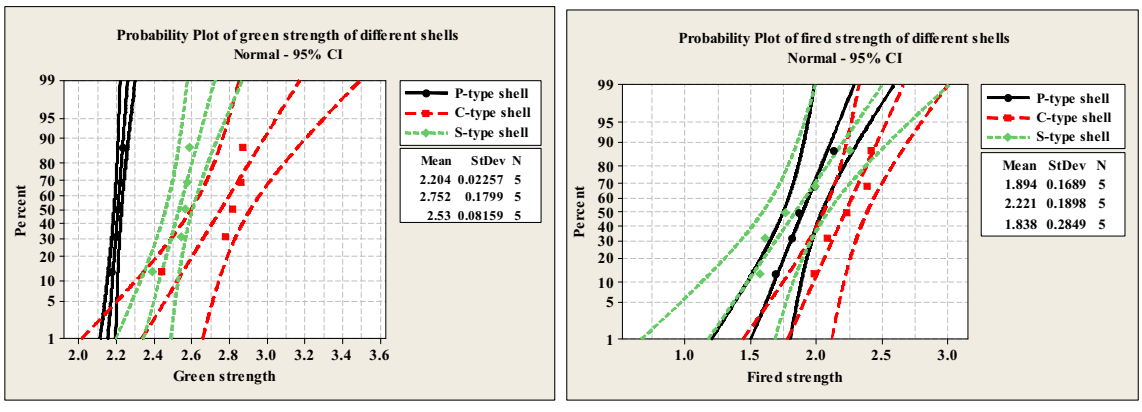

(a) **(b)**

Fig. 22 Probability plots of strength of ceramic shells (a) Green strength (b) Fired strength

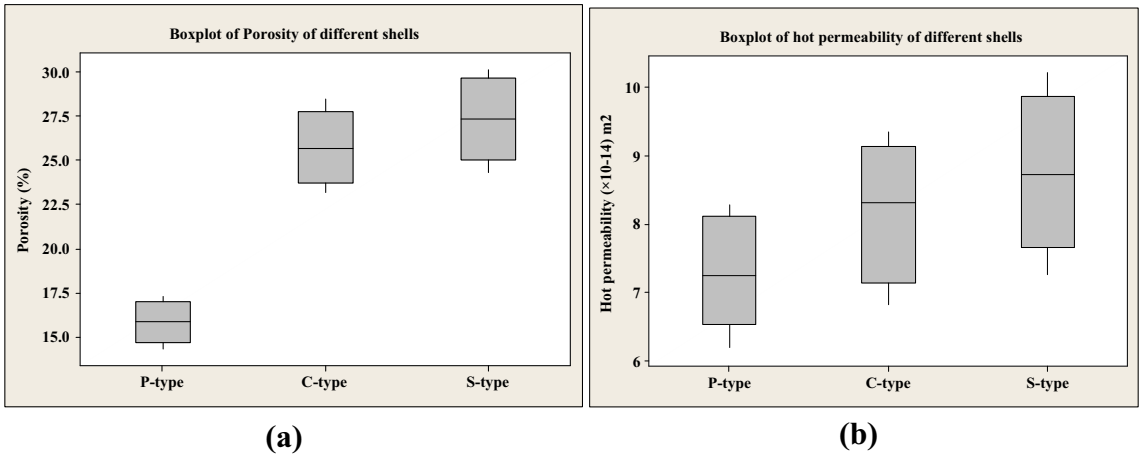

Fig. 23 Box plots for the analysis of characteristics of different shells (a) Porosity (b) Permeability

the median value of thicknesses of C-type shell was found to be the highest among all shells, which shows that increase in shell thicknesses at both regular section and sharp corners was comparatively high.

Further, the statistical analysis of the strengths of the different additives modified ceramic shells have been done, as shown by the probability plots in Fig. 22. The mean green and fired strengths of C-type shell were found to be maximum i.e. 2.752 MPa and 2.221 MPa, respectively. The mean green strength of P-type shell was lowest though polymer addition into the colloidal silica binder usually promotes green strength and elasticity of ceramic shell body system. This shows that C and S type shells have better bonding with the ceramic matrix due to their rough fibrous surface, which liquid polymer lacks.

The fired strength of S-type shell was lowest among all shells due to more porosity being found in it. The spread of green strength of C-type shell around the mean was found to be more than that of the other two shells which shows that the addition of coconut fibres to the ceramic shell severely increases the green strength of the shell as regards to other shells. Similarly, the spread of fired strength of S-type shell around the mean was found to be more than that of the other two shells, which shows that there is a severe decrease in the fired strength of the aforementioned shell with percent increase of saw dust in the shell.

Further, box plots for porosity and permeability of the shells were drawn (Fig. 23) and the data are presented in Table 8. It is seen that the median value of porosity and permeability of S-type shell is highest among all shells and the plots are almost symmetric about the median except for the hot permeability of C-type shell which is negatively skewed. Due to this higher porosity and hot permeability of S-type shell, more pores are there inside it thereby decreasing its fired strength.

4 Conclusions

The following conclusions are drawn from the present study:

- The density, viscosity and plate weight of the coconut fibre modified slurry were found to be more than that of

Table 8 Box plot data of porosity and permeability of different ceramic shells

Characteristic	Shell (mm)	P-type	C-type	S-type
Porosity (%)	Quartile Q1	14.685	23.695	24.995
	Median	15.87	25.66	27.35
	Quartile Q3	17.015	27.75	29.655
	Inter quartile range (IQR)	2.33	4.055	4.66
	Whiskers to:	14.31, 17.28	23.15, 28.43	24.28, 30.12
	N	5	5	5
Permeability ($\times 10^{-14}$) m^2	Quartile Q1	6.53	7.14	7.655
	Median	7.24	8.31	8.73
	Quartile Q3	8.11	9.14	9.865
	Inter quartile range (IQR)	1.58	2	2.21
	Whiskers to:	6.19, 8.28	6.82, 9.35	7.26, 10.22
	N	5	5	5

the polymer-modified and saw dust modified slurry for equal weight percentage of additives, which was followed by saw dust modified slurry. From the statistical analysis, the spread of C-type slurry (for all the slurry characteristics) was also found to be highest among the three slurries.

- The thickness of P-type, C-type and S-type ceramic shells increased with increase in percentage of additives. However, it was found that the median value of shell thickness of C-type ceramic shell was highest among all shell types at both regular sections and sharp corners for a five-layered shell system, which was followed by S-type ceramic shell.
- The shell thicknesses of C-type and S-type ceramic shells were overall 23.27% and 14.78% more than the P-type ceramic shell at regular section. Similarly, C-type and S-type ceramic shells showed 44.9% and 34.2% more thickness from that of P-type ceramic shell at sharp corners.
- The porosity and permeability of P-type, C-type and S-type ceramic shells increased with increase in percentage of additives. However, highest porosity and permeability was found in S-type ceramic shell which was followed by C-type ceramic shell.
- The flexural green strength of P-type shell increased with increase in percentage of liquid polymer up to 6%. However, it was found that the green strength of C-type and S-type ceramic shells increased with increase in additives from 2% to 5%, thereafter it decreased. Thus, the optimum amount of saw dust and coconut fibres to be added into the secondary ceramic slurries was limited to 5%. The variability of green strength of C-type ceramic shell around the mean was found to be highest, which was followed by S-type ceramic shell. The flexural fired strength of all shells exhibited a decreasing trend. However, C-type ceramic shell showed the most fired strength, followed by S-type ceramic shell.
- It was found from visual inspection that the cracks were generated on the C-type and S-type ceramic shells when the additive percentage was increased to 6%.
- The tensile strength was highest for the Al-7%Si alloy casting obtained from S-type ceramic shell which also showed least apparent porosity, whereas the same was found to be lowest for least porous P-type ceramic shell. The strength of the cast part obtained from S-type ceramic shell was more due to the higher cooling rate of casting in S-type ceramic shell i.e. 0.9 °C/s, whereas P-type and C-type ceramic shells exhibited casting cooling rates of about 0.7 °C/s (also appreciable) and 0.4 °C/s.

The present study shows that the saw dust and coconut fibre additions to the colloidal silica-based slurries significantly improved the properties of the IC ceramic shells at comparatively less cost and ultimately, the casting properties increased. It shows that saw dust and coconut fibres could be successfully added to the colloidal silica-based slurries for building the qualitative IC ceramic shells.

Acknowledgement The authors are grateful to MHRD, Government of India for providing financial support to the author for carrying out the research work.

References

1. Beeley PR, Smart RF (1995) Investment casting, 1st edn. The Institute of Materials, London
2. Jiang RS, Wang WH, Zhang DH, Wang ZQ Wall thickness monitoring method for wax pattern of hollow turbine blade. Int J Adv Manuf Technol. doi:10.1007/s00170-015-7561-9
3. Pattnaik SR, Karunakar DB, Jha PK (2012) Multi-characteristic optimization of wax patterns in the investment casting process using grey–fuzzy logic. Int J Adv Manuf Technol. doi:10.1007/s00170-012-4591-4
4. Pattnaik SR, Karunakar DB, Jha PK (2012) Developments in investment casting process - a review. J Mater Process Technol 212: 2332–2348
5. Roach PJ, Ponton CB (2013) Aqueous electrophoretic deposition as a method for producing an investment casting shell mould ceramic face-coat. Part 1: formation of a carbon-filled investment casting wax electrode material. Mater Sci. doi:10.1007/s10853-013-7562-8
6. Nadolski M, Konopka Z, Giewka M, Zyska A (2009) The influence of ceramic fibre on thermal expansion of moulding materials for investment casting technology. Arch Foundry Engg 9:1897–3310
7. Jia Q, Cui YY, Yang R (2006) A study of two refractories as mould materials for investment casting TiAl based alloys. J Mater Sci 41: 3045–3049
8. Jones S (1993) Improved sol based ceramic moulds for use in investment casting, Ph.D. Thesis, University of Birmingham, Edgbaston, UK
9. Harunl Z, Kamarudinl NH, Ibrahim M, Idris MI, Ahmad S. 2014 Reinforced Green Ceramic Shell Mould for Investment Casting Process. Advanced Materials Research Submitted: ISSN: 1662–8985, Vol. 1087, pp 415–419
10. Kline DM, Lekakh SN, Richards VL (2010). Improving Improving Casting Mold Permeability Using Graphite Particles. AFS Transactions American Foundry Society 159–165
11. Everhart W, Lekakh S, Richards V, Chen J, Li H, Chandrashekhara K (2013). Corner strength of investment casting shells, International Journal of Metal casting/Winter: 21–27
12. Yahaya B, Izman S, Idris MH, Dambatta MS (2016) Effects of activated charcoal on physical and mechanical propertiesof microwave dewaxed investment casting moulds. CIRP J Manuf Sci Technol. doi:10.1016/j.cirpj.2016.01.002
13. Fei CY, long XS, Jing T, juan X, yong CY (2011) Effect of particle size distribution on properties of zirconia ceramic mould for TiAl investment casting. Trans Nonferrous Met Soc China 21:s342–s347
14. Cheng X, Sun XD, Yuan C, Green NR, Withey PA (2012) An investigation of a TiAlO based refractory slurry face coat system for the investment casting of Ti-Al alloys. Intermetallics 29:61–69
15. Jin S, Liu C, Lai X, Li F, He B (2016) Bayesian network approach for ceramic shell deformation fault diagnosis in the investment casting process. Int J Adv Manuf Technol. doi:10.1007/s00170-016-8795-x
16. Ferreira JC, Mateus A (2003) A numerical and experimental study of fracture in RP stereolithography patterns and ceramic shells for investment casting. J Mater Process Tech 134(1):135–144

17. Ku H, Cardona F, Trada M (2012) Flexural properties of sawdust-reinforced epoxy composites post-cured in microwaves. J Compos Mater. doi:10.1177/00219983
18. Kumaoka S (2000) Method of preparing porous ceramics provided with amorphous pore surfaces. US Patent No. 6042763A (March 28)
19. Naveen PNE, Raju TD (2013) Evaluation of mechanical properties of coconut coir fiber reinforced polymer matrix composites. J Nano Research 24:34–45
20. Van Dam JEG, Van Den Oever MJA, Teunissen W, Keijsers ERP, Peralta AG (2004) Process for production of high density/high performance binderless boards from whole coconut husk. Part 1: lignin as intrinsic thermosetting binder resin. Industrial Crops Products 19:207–216
21. Brahmakumar M, Pavithran C, Pillai RM (2005) Coconut fibre reinforced polyethylene composites: effect of natural waxy surface layer of the fibre on fibre/matrix interfacial bonding and strength of composites. Composites Sci Technol 65:563–569
22. ASTM standard method D2395-07a, Specific gravity of wood and wood-based materials
23. ASTM standard method E1755–01, Determination of Ash Content of Particulate Wood Fuels
24. Horisawa S, Sunagawa M, Tamai Y, Matsuoka Y, Miura T, Terazawa M (1999) Biodegradation of nonlignocellulosic substances II: physical and chemical properties of saw dust before and after use as artificial soil. J Wood Sci 45:492–497
25. Sidhu BS, Kumar P, Mishra BK (2008) Effect of slurry composition on plate weight in ceramic shell investment casting. J Mater Eng Performance 17:489–498
26. ASTM standard method C20, Standard test methods for apparent porosity, water absorption, apparent specific gravity, and bulk density of burned refractory brick and shapes by boiling water
27. Amira S, Dube D, Tremblay R (2011) Method to determine hot permeability and strength of ceramic shell moulds. J Mater Process Technol 211:1336–1340
28. Hann SW (2009) Effect of oil palm fibre addition on the mechanical properties of shell mould investment casting, Master's Thesis, Faculty of Mechanical Engineering, University of Technology Malaysia
29. Vavrina CS, Armbrester K, Arenas M and Pena M (2002) Coconut Coir as an Alternative to Peat Media for Vegetable Transplant Production, SWFREC Station Report - VEG 96.7, Southwest Florida Research and Education Center, P.O. Drawer 5127 Immokalee, FL 33934
30. Xu M (2015) Characterization of investment shell thermal properties, doctoral thesis, metallurgical engineering, Missouri university of science and technology. University in Rolla, Missouri
31. Pattnaik SR, Karunakar DB and Jha PK (2015) A novel method of increasing ceramic shell permeability and optimizing casting shrinkage and tensile strength of the investment cast parts, J Engineering Manufacture 1–12, DOI:10.1177/0954405415606386
32. Joseph K, Filho RDT, James B, Thomas S, Carvalho LHD (1999) A review on sisal fiber reinforced polymer composites. Revista Brasileira de Engenharia Agrícola e Ambiental 3(3):367–379
33. Li Z, Wang L, Wang X (2007) Cement composites reinforced with surface modified coir fibers. J Comp Mater 41(12):1445–1457
34. Chang CJ, Li DC, Huang YH, Chen CC (2015) A novel gray forecasting model based on the box plot for small manufacturing data sets. Appl Math Comput 265:400–408